Geometrically engineered organoid units and their assembly for pre-construction of organ structures (F)

Ayaka Kadotani,[1] (iD) Gen Hayase,[2,a] (iD) and Daisuke Yoshino[1,3,a] (iD)

AFFILIATIONS

[1]Department of Biomedical Engineering, Graduate School of Engineering, Tokyo University of Agriculture and Technology, 2-24-16 Naka-cho, Koganei, Tokyo 184-8588, Japan
[2]Research Center for Electronic and Optical Materials, National Institute for Materials Science, 1-1 Namiki, Tsukuba, Ibaraki 305-0044, Japan
[3]Division of Advanced Applied Physics, Institute of Engineering, Tokyo University of Agriculture and Technology, 2-24-16 Naka-cho, Koganei, Tokyo 184-8588, Japan

[a]Authors to whom correspondence should be addressed: gen@aerogel.jp and dyoshino@go.tuat.ac.jp

ABSTRACT

Regenerative medicine is moving from the nascent to the transitional stage as researchers are actively engaged in creating mini-organs from pluripotent stem cells to construct artificial models of physiological and pathological conditions. Currently, mini-organs can express higher-order functions, but their size is limited to the order of a few millimeters. Therefore, one of the ultimate goals of regenerative medicine, "organ replication and transplantation with organoid," remains a major obstacle. Three-dimensional (3D) bioprinting technology is expected to be an innovative breakthrough in this field, but various issues have been raised, such as cell damage, versatility of bioink, and printing time. In this study, we established a method for fabricating, connecting, and assembling organoid units of various shapes independent of cell type, extracellular matrix, and adhesive composition (unit construction method). We also fabricated kidney tissue-like structures using three types of parenchymal and interstitial cells that compose the human kidney and obtained findings suggesting the possibility of crosstalk between the units. This study mainly focuses on methods for reproducing the structure of organs, and there are still issues to be addressed in terms of the expression of their higher-order functions. We anticipate that engineering innovation based on this technique will bring us closer to the realization of highly efficient and rapid fabrication of full-scale organoids that can withstand organ transplantation.

INTRODUCTION

The development of three-dimensional (3D) culture systems, organoids, has been the most exciting advance in medical and biological fields in the last two decades since the invention of iPS cells.[1–6] This organoid system has enabled the modeling of genetic, degenerative, and cancer diseases that were difficult to reproduce *in vitro*[7–11] and has been expected to lead to innovative advances in establishing medical treatments. Organoids can express the higher-order functions of organs,[12] but are currently limited to a few millimeters in size, referred to as "mini-organs" are called. Therefore, one of the ultimate goals of regenerative medicine, "organ replication and transplantation using organoids," faces a major obstacle.

Currently, 3D bioprinting is the most promising method for producing artificial tissue that can be used as organs for transplantation. Extrusion-based bioprinting (EBB), in which a solution containing living cells, bioink, is extruded and layered in a 3D space such as a 3D printer, is a mainstream method.[13] EBB has the advantage of being able to form complex structures, including internal architecture, without the need to prepare molds with cell-dense solutions as bioinks.[14] Conversely, problems with EBB include cellular damage due to pressure and shear forces during bioink ejection, the difficulty of developing bioinks with appropriate mechanical, structural, and biological properties, and the long time required to print full-size organs.[15–17] Volumetric bioprinting (VBP), unlike conventional methods (i.e.,

layer-by-layer stacking), creates an object by photo cross linking the resin by exposing it to a calculated two-dimensional (2D) light pattern while rotating a transparent container.[18] As a result, it takes only a few seconds to a few minutes to fabricate a model, regardless of size. The features of short fabrication time and nozzle-less fabrication do not affect cell viability and functionality and provide high resolution (up to tens of micrometers).[19] Hence, VBP is a new and promising technique that overcomes several of EBB's limitations. However, it is difficult to precisely control the position and density distribution of cells in the pre-cured gel with current methods,[19,20] and it is expected to be challenging to construct full-size organs composed of different cells and extracellular substrates. Therefore, it is desirable to develop a technique for artificially constructing organ-size 3D tissues with high efficiency and yield.

To address these current problems, a method of 3D tissue engineering using organoid building blocks (OBBs), i.e., stacking OBBs such as spheroids and organoids to reproduce organ-specific functions, has been developed.[21] The stacking of organoids and spheroids ranging in size from several hundred μm^3 to 1 mm^3 is expected to significantly reduce the printing time currently required for the spatial arrangement of single cells, bringing us closer to the rapid construction of human tissues. In particular, the OBB has recently been introduced into a 3D bioprinter, enabling large-scale organoid-like structures, assembloid, by realizing rapid spatial arrangement.[21–24] Although this technology solves the heterogeneity of iPS cell-derived organoids, more is needed to address the limitations of the types of bioinks, the size of the OBBs that can be used, the complicated spatial arrangement due to the basic shape of the block, such as a sphere, and the changes in bioink properties associated with printing due to the use of a 3D bioprinter.

In contrast, we conceptualize the establishment of a method to assemble organoid units of various shapes that are pre-divided into basic organ elements like construction toys (unit construction method). The unit construction method has several advantages over conventional technologies. First, there are no limitations on the types of extracellular matrix (ECM) that are used, and it is cell-friendly by avoiding damage from pressure, etc., because it does not involve extrusion molding like a 3D printer. Second, the method allows us to construct organoids containing multiple cells and ECMs with high efficiency by fabricating each unit from different cells and ECMs and then assembling them. Furthermore, we can easily reproduce complex structures by combining units that are not limited to simple geometries, such as spheres and sheets. This method leads to a highly efficient and rapid technique for producing full-scale organoids that can survive organ transplantation. In the future, we envision the production of organoids of transplantable size. In particular, we are focusing on the construction of full-size kidney organoids as one of the treatment options for kidney diseases that are difficult to cure with drugs. Here, we show our method for fabricating organoid units with six different shapes and the cellular dynamics inside the units when stacked, as well as the results of forming and assembling the units using three types of parenchymal and interstitial cells that compose the human kidney.

RESULTS AND DISCUSSION
Fabrication of organoid units with various geometries

We first selected and fabricated the organoid units with the geometry necessary to reproduce the nephrons and other structures in the human kidney. We confirmed that we had no problems releasing the organoid units with various shapes from the molds, and could fabricate them with constant reproducibility [Figs. 1(a) and 1(b), supplementary Fig. 1]. Organoid units made with MDA-MB-231 cells contracted in size as they matured [Fig. 1(c)]. Previous studies have also reported this phenomenon, which is partly due to actomyosin contractility,[25] typical of highly invasive or motile cell types. Notably, even organoids with complex shapes contracted while maintaining their overall shape [Figs. 1(d)–1(i)]. The bead ring-shaped units also showed their contraction without rupture of their respective connecting parts.

Cell proliferation inside and on the surface of the organoids was observed as the culture duration progressed [Figs. 2(a)–2(f)]. As the organoid units, which are thicker than the sheet types [Fig. 2(d)], matured, the cells inside them became denser and underwent cell death. This is caused by the dense cellular area on the organoid surface layer, which acts like a shell and blocks the oxygen and nutrient supply to the inner cells.[26,27] This notion is supported by the results of an evaluation of cell death within the 2 mm-diameter spherical organoid units stained with Hoechst, Annexin V (a marker of apoptosis), and Ethidium homodimer III (a marker of necrosis). The percentage of Ethidium homodimer III-positive cells increased with the number of days in culture for both types of organoid units [MDA-MB-231, Figs. 2(g) and 2(h); HRGEpCs, Figs. 2(i) and 2(j)]. In contrast, the percentage of Annexin V-positive cells did not change with culture duration [Fig. 2(j)]. Cell death within organoids is a common problem in previous organoid studies. It can be circumvented by properly arranging supply channels such as the vascular networks.[28,29] This study allows us to easily fabricate organoid units that reproduce the vascular system, as described below. By placing these units inside during assembly, a large-scale organoid that can be cultured for a long period of time is expected to be constructed.

We then assembled the various organoid units to evaluate a unit construction method. The substrate, collagen solution, was applied to the area with a micropipette and incubated for 2–5 min to allow the units to bond and stack [Fig. 3(a)]. Once the four cylindrical units were joined together to form a structure, we were able to grab one end of the structure with tweezers and pull it up, holding the structure in place without breaking it apart [Figs. 3(b) and 3(c), supplementary Movie 1]. Even rectangular units could be easily glued together [Fig. 3(d)], and more units could be stacked on top of the glued units [Fig. 3(e)]. The composite of the stacked units did not collapse when shaken (supplementary Movies 2 and 3). After assembly, continued culture is expected to induce proliferation and organization of cells within the units, leading to crosstalk between the units [Fig. 3(f)]. However, there are still some problems with the bonding. In this study, the ECM solution that acts as an adhesive is applied by a micropipette, which results in a large loss due to the inability to apply the solution in a spot manner. This causes a large displacement in the stacking of multiple units. Thus, it suggests that the realization of micro-spot bonding and precise stacking (e.g., micromanipulation system) is necessary for the future construction of organ structures.

Construction and assembly of kidney glomerular tissue-like organoid units

The use of easy-to-handle cancer cell lines is suitable for validating the production of living parts of various shapes for full-scale
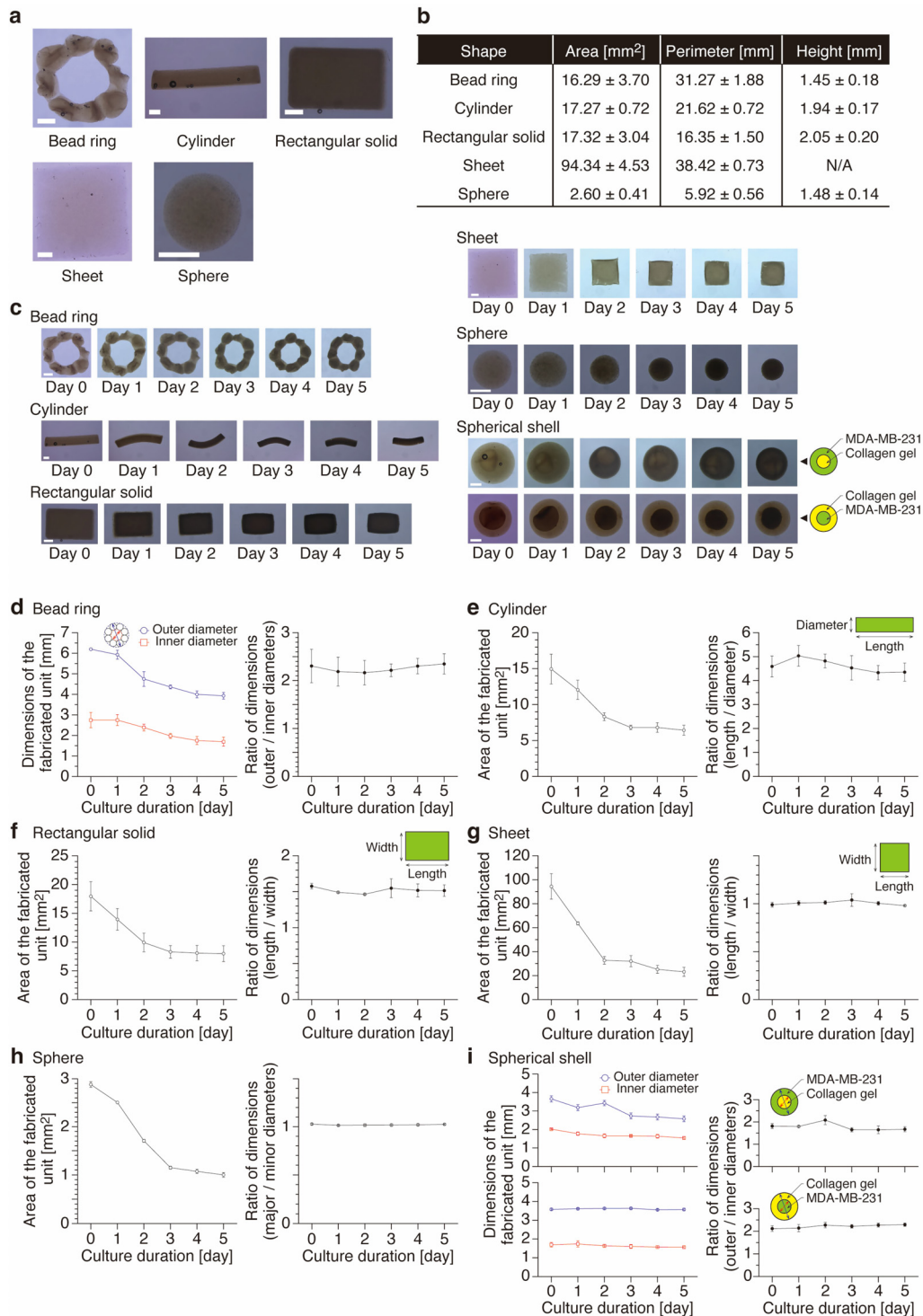
FIG. 1. Fabrication of organoid units with various geometries. (a) MDA-MB-231 organoid units immediately after fabrication with typical shapes ($n = 5$). Scale bars, 1 mm. (b) Table of shape reproducibility in organoid fabrication immediately after they were fabricated (day 0) (mean $\pm$ SD, $n = 5$). (c) Time-sequenced brightfield images of MDA-MB-231 organoid units of various geometries ($n = 3$). Scale bars, 1 mm. (d)–(i) Dimensional changes of MDA-MB-231 organoid units of various shapes and their ratios with culture duration [(d) bead ring; (e) cylinder; (f) rectangular solid; (g) sheet; (h) sphere; and (i) spherical shell, mean $\pm$ SD, $n = 3$]. For the spherical shells, we evaluated the case where a layer of cells was placed on the outside and inside, respectively.

organoid construction. However, it is a considerable leap in research and development steps to construct something that functions as an organ (especially a kidney). Here, we examined the validity of our proposed method (unit construction) by constructing and assembling units with organ-like structures under a tri-culture of parenchymal and interstitial cells (i.e., renal glomerular epithelial cells, mesangial cells, and vascular endothelial cells) that consist of the kidney glomerulus. Tri-cultured organoid units exhibited a tissue-like structure, where HRGEpCs were complexly intertwined around HUVECs, which formed a vascular network, and NHMCs were interspersed around them [Fig. 4(a)]. These findings are supported by the co-localization of marker proteins of each cell type [i.e., Pearson's correlation coefficient; Fig. 4(b)]. Integrating these two sets of data [Figs. 4(a) and 4(b)] provides a rough outline of the internal structure in the fabricated unit. Compared to the histological structure of a normal human kidney,[30–32] the morphology and distribution of NHMCs and HUVECs in the fabricated organoid unit were similar to those of mesangial cells and endothelial cells in the renal glomerulus. However, HRGEpCs, which become podocytes in a normal kidney, were in close spatial proximity to HUVECs but did not form a membrane-like structure around them. The reason for this may be that the tissue did not mature well under the culture conditions in this study due to the lack of orientation of the units. We should further investigate the challenges in structural mimicry (i.e., the formation of membrane-like structures by HRGEpCs) while analyzing the spatial relationships of cells in more detail in the future.

The vascular network formed by the HUVECs decreased with the progression of the culture, and by day 5, the internal network had almost disappeared [Fig. 4(c)]. This is most likely due to the fact that the network was recognized as unnecessary because the units were cultured statically. This notion is supported by reports that turnover of the vascular network is induced when the culture medium is not perfused.[33,34] After the tri-cultured organoid units were bonded to each other with a substrate solution containing interstitial cells (HUVECs), the vascular network formed by the HUVECs seemed to connect the two units [Fig. 4(d)]. Crosstalk between units will be possible if the structures with stacked units are cultured under appropriate conditions, including perfusion of the medium into the vascular network, and we can expect the stacked structures to mature as tissues. However, the vascular network did not function properly and continued to mature, and it began to disappear after the third day. In order to maintain long-term culture while inducing crosstalk between cells in multiple units, a hierarchical vascular network that functions as a supply channel for oxygen and nutrients is essential. An open question for the future is how to maintain the vascular network formed within the organoid complex and to mature it into a hierarchical structure.

Assembly of organoid units with different geometries, aiming to construct a complex structure

To reproduce the complex structure of human organs, we need to combine organoid units with different shapes. Finally, we investigated the scalability of the proposed method by assembling bead-ring-shaped and cylinder-shaped units. Using tweezers, we gently lifted the bead ring-shaped unit and inserted the cylinder-shaped unit into its central space [Fig. 5(a)]. The contact points between the units were bonded with collagen solution or protein solution (mixture of collagen and Matrigel), and the complexes were cultured for 5 days. For the

practice, we started by assembling organoid units prepared with MDA-MB-231 cells, which are easy to handle [Figs. 5(b) and 5(c)]. During the 5-day culture, we observed that the units did not peel off from each other, but gradually contracted while maintaining their shape. As with other results, the cells inside the organoid units gradually underwent cell death as the culture duration progressed. Although it is difficult to see in the bright field observation results [Fig. 5(b)], the fluorescence imaging results [Fig. 5(c)] show that the spherical beads were arranged in a 3D manner in front of and behind the cylinder-shaped units. We were also able to construct a 3D structure in the same way using organoid units mimicking kidney glomerular tissue (i.e., organoids tri-cultured with NHMCs, HUVECs, and HRGEpCs) [Fig. 5(d)]. Summarizing the above-mentioned results, we can conclude that the proposed method has the potential to replicate complex human organ structures by assembling organoid basic units.

Our proposed unit construction method can construct tissue-like structures by fabricating and assembling organoid units of various shapes and sizes. The unit construction method is completely different from 3D bioprinting (i.e., it does not require bioink) and has no limitations on the types of ECMs that can be used. We can fabricate units using a similar protocol even in an environment with different cells and ECMs, and we can construct organoids containing multiple cells and ECMs with high efficiency by simply assembling them. Of course, a detailed micromanipulation system is required for their assembly, but this is suitable for constructing organoids that mimic real organs, which are complex and large structures, because it is also possible to combine units with different geometries. Cell viability can also be maintained at a high level by adequately arranging the vascular network that supplies oxygen and nutrients inside under appropriate conditions. Our approach is similar in some respects to the developmental process of tissues and organs because we subdivide the structure of the target organ into elements (units), utilize self-organization of cell clusters at the unit level, and finally assemble them. In contrast, conventional bioprinting technologies[21,35,36] have the advantage of being able to arrange cell clusters in space, but still need to solve the issues of bioink development and its influence on cell viability and function, as well as the time required to construct full-scale organoids. In addition, in cases where multiple cell types are used in bioprinting, it is easy to foresee various obstacles to optimizing printing conditions. In general, however, we believe that the greatest challenge for both conventional bioprinting and our method is the expression of higher-order functions in the target organs[37–39] in order to realize the construction of transplantable organoids. Furthermore, we may have to mimic the mechanical properties of tissues, especially the interstitium, in the future, considering that cells sense the surrounding mechanical field, including the extracellular matrix, and change their functions.[40–43]

CONCLUSIONS

In conclusion, we have proposed a method for fabricating and assembling organoid units of various shapes with a size of a few mm as basic elements for the realization of full-scale implantable organoids in the future (Fig. 6). Our method is not limited by the ECM types and organoid unit size because it does not use a 3D bioprinter. Therefore, the users can choose the ECM suitable for the organoid unit to be constructed. Moreover, there is no restriction on the adhesive used in our method, so by selecting the appropriate adhesive, it is possible to fabricate large constructions such as assembloids at high speed, which is expected to achieve the "highly efficient and high-volume 3D tissue
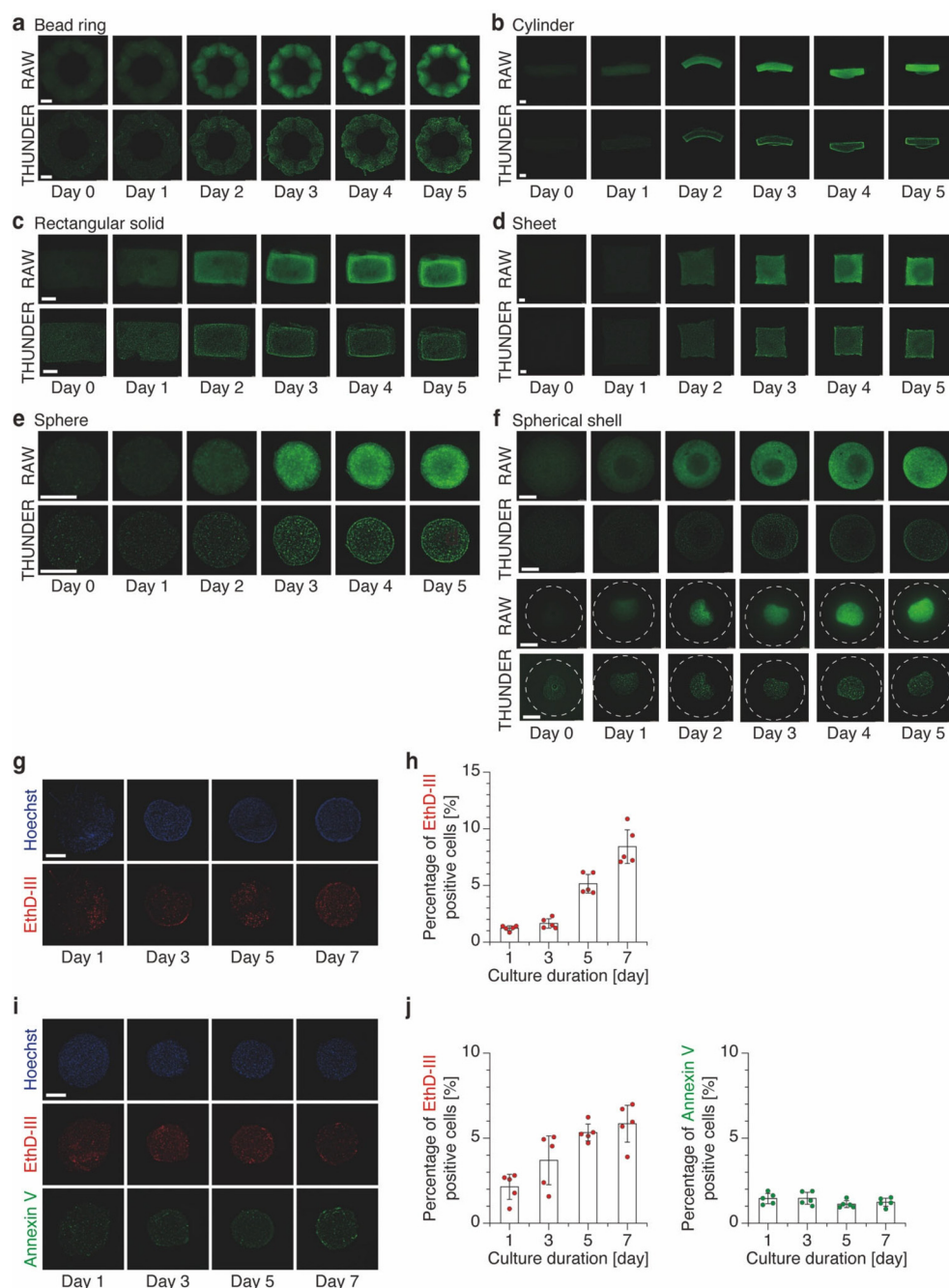
FIG. 2. Cell dynamics inside the fabricated organoid units. (a)–(f) Live fluorescence images of MDA-MB-231 organoid units, expressing GFP in the cytoplasm, with various geometries [(a) bead ring; (b) cylinder; (c) rectangular solid; (d) sheet; (e) sphere; and (f) spherical shell, mean $\pm$ SD, $n = 3$]. *Upper row*: wide-field fluorescence images (raw data), and *lower row*: images processed by the THUNDER imaging system with instant computational clearing (ICC) and extended depth of field (EDF). Dashed lines indicate the outline of the outer shell formed by the collagen gel (f). Scale bars, 1 mm. (g) Representative results of live/dead assays for MDA-MB-231 organoid units ($n = 5$). The MDA-MB-231 cells express GFP in their cytoplasm, and we therefore performed necrosis detection using Ethidium homodimer III (EthD-III). Scale bars, 500 μm. (h) Quantification of EthD-III-positive cells in the organoid units (mean $\pm$ SD, $n = 5$). The quantified results indicate the percentage of EthD-III-positive cells per cell number (EthD-III/Hoechst ratio). (i) Representative results of live/dead assays for organoid units prepared with HRGEpCs ($n = 3$). Scale bars, 500 μm. (j) Quantification of EthD-III-positive and Annexin-V positive cells in the organoid units (mean $\pm$ SD, $n = 5$). The quantified results indicate the percentage of EthD-III-positive and Annexin V-positive cells per cell number (EthD-III/Hoechst ratio and Annexin V/Hoechst ratio).

fabrication" required for transplantation medicine. However, it is essential to introduce manipulation techniques such as micromanipulation because precise movements are required to assemble organoid units.

METHODS

Cell culture

An easy-to-handle cancer cell line was used to validate the feasibility of fabricating the organoid units and their assembly. Green fluorescent protein (GFP)-labeled human breast adenocarcinoma cell line (MDA-MB-231; AKR-201, Cell Biolabs, San Diego, CA, USA) was cultured with Dulbecco's modified eagle medium (DMEM; 31600-034, Gibco, Thermo Fisher Scientific, Waltham, MA, USA) containing 10% heat-inactivated fetal bovine serum (FBS; S1810, Biowest, Nuaillé, France) and 1% penicillin-streptomycin (P/S; 15140-122, Gibco). This cell line has been used in our previous studies to form spheroids with collagen substrates.[25,44] Three types of human primary cells were also used to validate the construction of organ-like structures by co-culturing parenchymal and interstitial cells: human renal glomerular epithelial cells (HRGEpCs; 942-05n, Cell Applications, San Diego, CA, USA), human glomerular mesangial cells (NHMCs; ACBRI127, Cell Systems, Kirkland, WA, USA), and human umbilical vein endothelial cells (HUVECs; 200-05n, Cell Applications). The primary cells were cultured with Medium 199 (31100-035, Gibco) containing 5% FBS, 1% P/S, 10 μg/L human basic fibroblast growth factor (bFGF; GF-030-3, AUSTRAL Biologicals, San Ramon, CA, USA), 10 μg/L human epidermal growth factor (hEGF; E9644, Sigma-Aldrich, St. Louis, MO, USA), 1% ITS-X supplement (094-06761, Fujifilm Wako Pure Chemical Corp., Osaka, Japan), 36 μg/L hydrocortisone (50-23-7, MP Biomedicals, Irvine, CA, USA), and 4 ng/L 3,3',5-triiodo-L-thyronine sodium salt (T6397, Sigma-Aldrich). The cells were cultured in a 75 cm^2 flask (658175, Greiner Bio-One, Kremsmünster, Austria) precoated with/without 0.1% bovine gelatin solution (G9391, Sigma-Aldrich) until reaching 90% confluence. Primary cells from the fifth to ninth passages were used for experiments in this study.

Mold processing

Monolithic porous bulk material with superhydrophobicity (boehmite nanofiber-polymethylsilsesquioxane; BNF-PMSQ)[44] was processed using a CNC milling machine (monoFab SRM-20 or MDX-50, Roland DG, Shizuoka, Japan) to manufacture molds for various shapes of organoids. We fabricated bead ring, cylinder, rectangular solid, cubic, and sheet-shaped molds in addition to the spherical one[25,44] (supplementary Fig. 2). The mold models were created in a 3D-CAD (SolidWorks, Dassault Systémes SOLIDWORKS Corp., Waltham, MA, USA) and then exported in STL format, from which the processing paths were coded by CAM software (SRP Player, Roland DG). Processing was performed in two stages, roughing and finishing, to prepare the surface of the monolithic porous material and make it superhydrophobic (supplementary Table 1). Polytetrafluoroethylene (PTFE) was used as the mold material when necessary.

Organoid unit fabrication

To validate the feasibility of fabricating the organoid units and their assembly, the MDA-MB-231 cells or HRGEpCs were harvested after reaching 90% confluence with 0.25% trypsin-EDTA (25200-072, Gibco) or 0.05% trypsin-EDTA (25300-062, Gibco), respectively. The cells were then resuspended in the culture medium at a concentration of 5.0×10^7 cells/ml. Cell-suspended collagen solution [4.0 mg/ml; native collagen acidic solution (IAC-50, KOKEN, Tokyo, Japan), 10× DMEM, 10 mM NaHCO$_3$, 10 mM HEPES-NaOH (pH7.5), and the cell suspension] was prepared on ice to give the final concentration of 5.0×10^6 cells/ml. The cell-suspended collagen solution was then dispensed onto the sterilized molds in a predetermined amount and order (Fig. 7). The dispensed solution was allowed to stand still in a CO$_2$ incubator (37 °C in a 100% humidified atmosphere of 5% CO$_2$) for 30–60 min. After gelation, the primary organoid block was transferred to a 35 mm diameter dish (3000-035, AGC Techno Glass, Shizuoka, Japan) by dropping a small amount of medium to cover it, poking it with the tip end of a micropipette to float it, and then adding more medium to pour it in. The units were incubated and matured for up to 5 days while being observed under a stereomicroscope (SZX16, Olympus, Tokyo, Japan) or a fluorescence imaging system (THUNDER Imaging System, Leica Microsystems, Wetzlar, Germany).

To validate the construction of organ-like structures with the units in tri-culture, the HRGEpCs, NHMCs, and HUVECs were harvested after reaching 90% confluence with 0.05% trypsin-EDTA and resuspended in the culture medium at a concentration of 5×10^8 cells/ml. Cell-suspended protein solution [4.5 mg/ml Matrigel (Matrix for Organoid Culture, 356255, Corning, Corning, NY, USA), 1.5 mg/ml native collagen acidic solution, 10× DMEM, 10 mM NaHCO$_3$, 10 mM HEPES-NaOH (pH7.5), and the cell suspensions] was prepared on ice to give the final concentrations of 0.5×10^7 cells/ml (HRGEpCs and NHMCs) and 4.0×10^7 cells/mL (HUVECs), respectively (i.e., HRGEpCs:NHMCs:HUVECs = 1:1:8). Tri-cultured organoid units, similar to MDA-MB-231 units, were formed and gelatinized with the prepared solution. They were then transferred to 48-well plates (VTC-48, AS ONE Corp., Osaka, Japan) and cultured for 7 days using OncoPro medium (A5701201, Gibco) supplemented with 1% P/S, 10 μg/L bFGF, and 10 μg/L hEGF.

Organoid unit assembly (unit construction)

The units were first transferred to an empty tissue culture dish using a micro spatula (6-524-01, AS ONE Corp.) or tweezers for block-to-block assembly. We applied 5–10 μl of adhesive to the area to be bonded with a micropipette, stuck the units together, and incubated for 2–5 min. Collagen solution [2.5 mg/ml; native collagen acidic solution, 10× DMEM, 10 mM NaHCO$_3$, 10 mM HEPES-NaOH (pH7.5), and ultrapure water] was used as the adhesive for bonding MDA-MB-231 units, and protein solution [4.5 mg/ml Matrigel, 1.5 mg/ml native collagen acidic solution, 10× DMEM, 10 mM NaHCO$_3$, 10 mM HEPES-NaOH (pH7.5), and the cell suspension (HUVECs; final concentration, 1.0×10^6 cells/ml)] was used for bonding tri-cultured units. After bonding, the assembled units were transferred to the 35 mm diameter dish filled with the culture medium using a medicine spoon to continue incubation.

Antibodies

The sheep polyclonal anti-nephrin antibody (Cat# AF4269) was purchased from R&D Systems (Minneapolis, MN, USA). The mouse
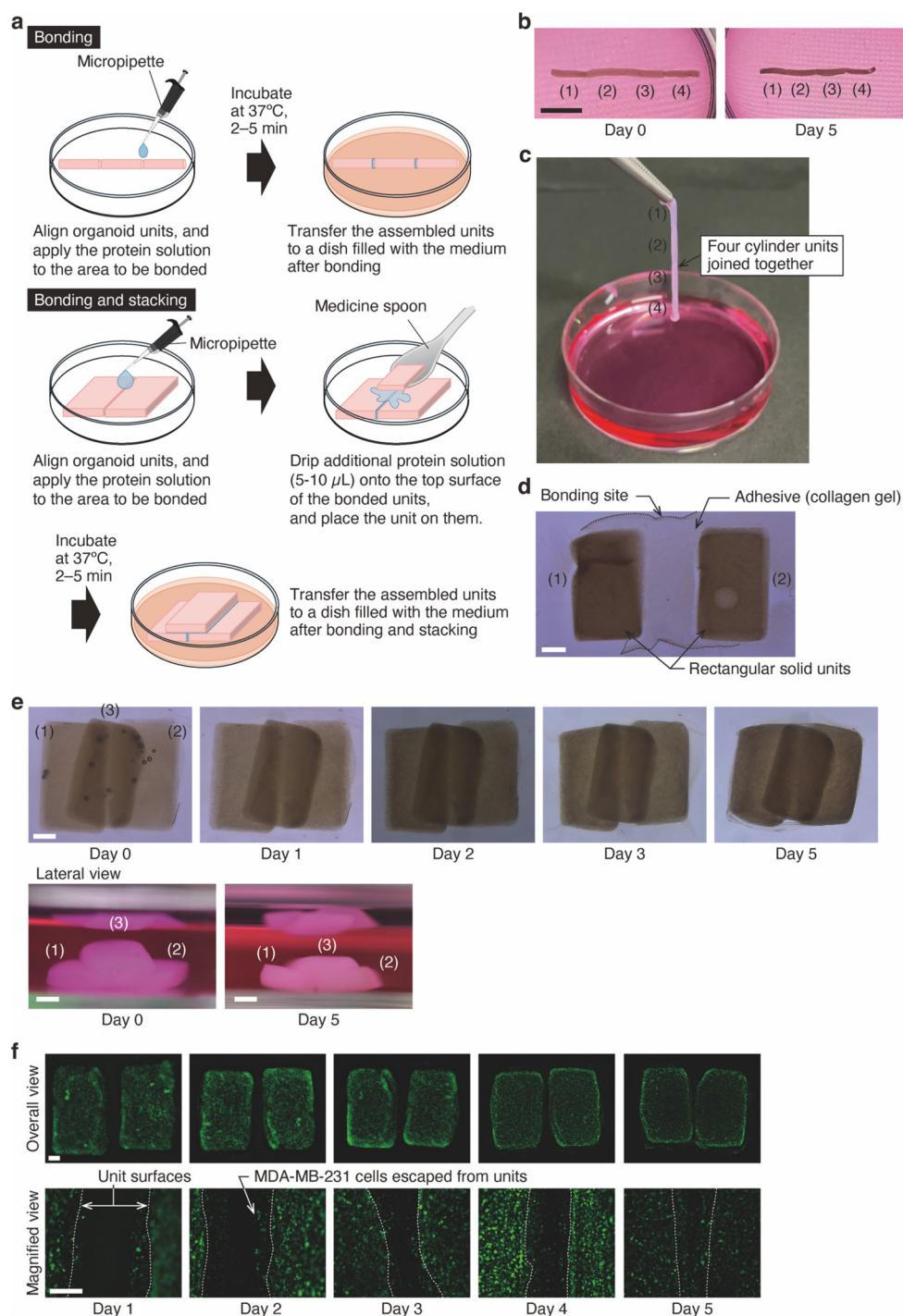
FIG. 3. Assembly of organoid units with various geometries. (a) Overview of bonding and stacking methods for organoid units. (b) Four-cylinder MDA-MB-231 organoid units bonded with collagen solution. Scale bar, 10 mm. (c) The jointed units can be pinched and lifted with tweezers without breaking into shreds. (d) Two rectangular solid MDA-MB-231 organoid units bonded together. Scale bar, 1 mm. (e) Three rectangular solid units were bonded and stacked and showed no signs of dissociation during the five-day culture period. The stacking of the units was confirmed from the lateral view. Scale bar, 1 mm. (f) Live fluorescence images of cellular dynamics around the bonding area between the units (*upper row*: overall view. Scale bar, 1 mm; *lower row*: magnified view. Scale bar, 500 μm). From day 1, cells that escaped from the units began to migrate into the collagen gel at the bonding area. Around day 4, cells proliferated at the bonding area, and the units connected in a cell cluster. The images were processed by the THUNDER imaging system with instant computational clearing (ICC) and extended depth of field (EDF). All data shown are representative of three independent experiments.
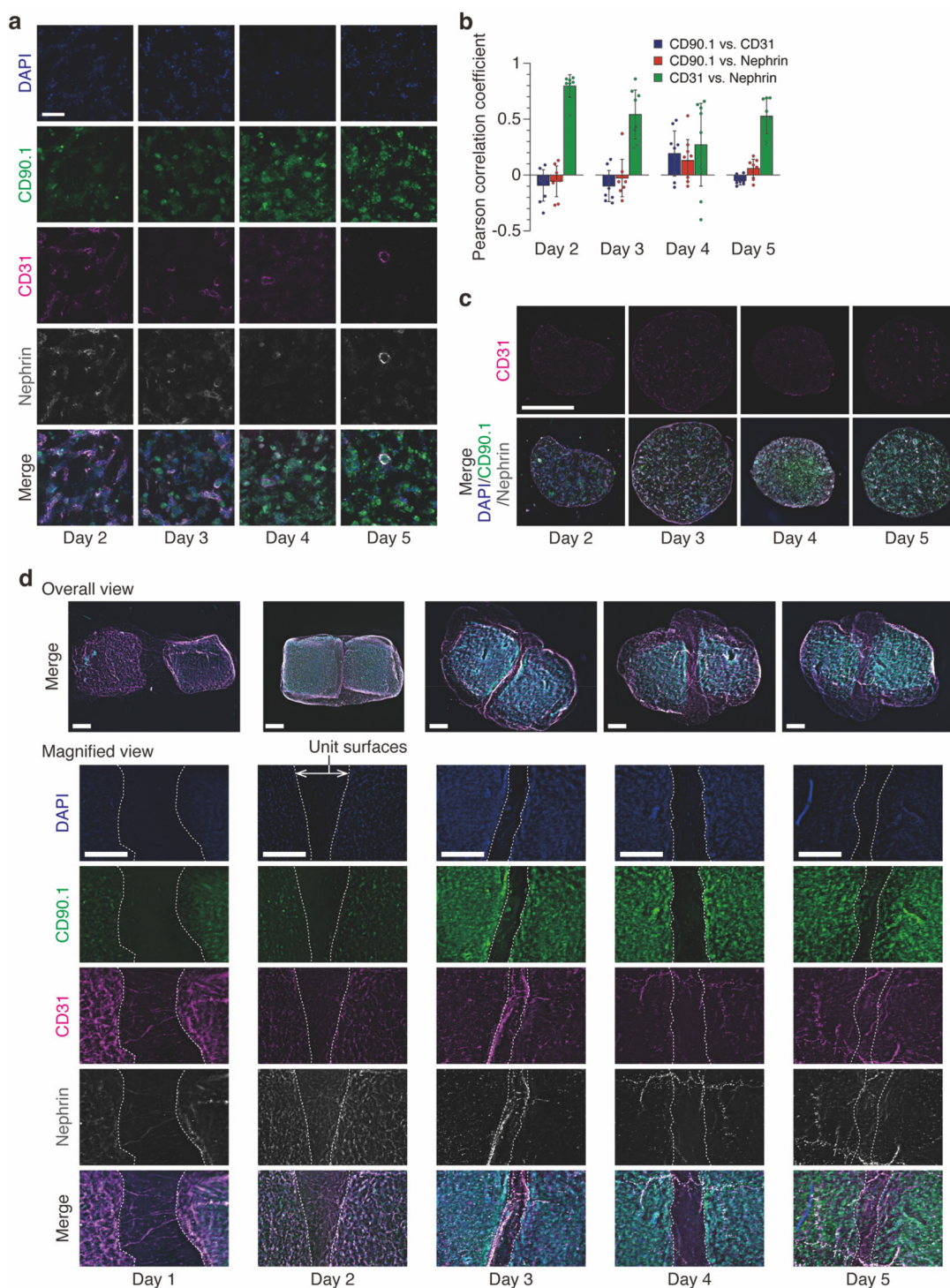
FIG. 4. Construction and assembly of human kidney glomerular tissue-like organoid units. (a) Fluorescence-stained frozen sections of tri-cultured spherical organoid units ($n = 3$). Each marker protein is stained on three cell types: NHMCs (CD90.1), HUVECs (CD31), and HRGEpCs (Nephrin). Scale bar, 50 μm. (b) Changes over culture duration in co-localization of marker proteins (mean $\pm$ SD, $n = 3$; 8; or 9 images). (c) Overall view of fluorescence-stained frozen sections of tri-cultured spherical organoid units ($n = 3$). Scale bar, 500 μm. (d) Representative fluorescence-stained images of cellular dynamics around the bonding area between the tri-cultured cubic organoid units ($n = 3$, *upper row*: overall view. Scale bar, 1 mm; *lower 5 rows*: magnified view. Scale bar, 500 μm).
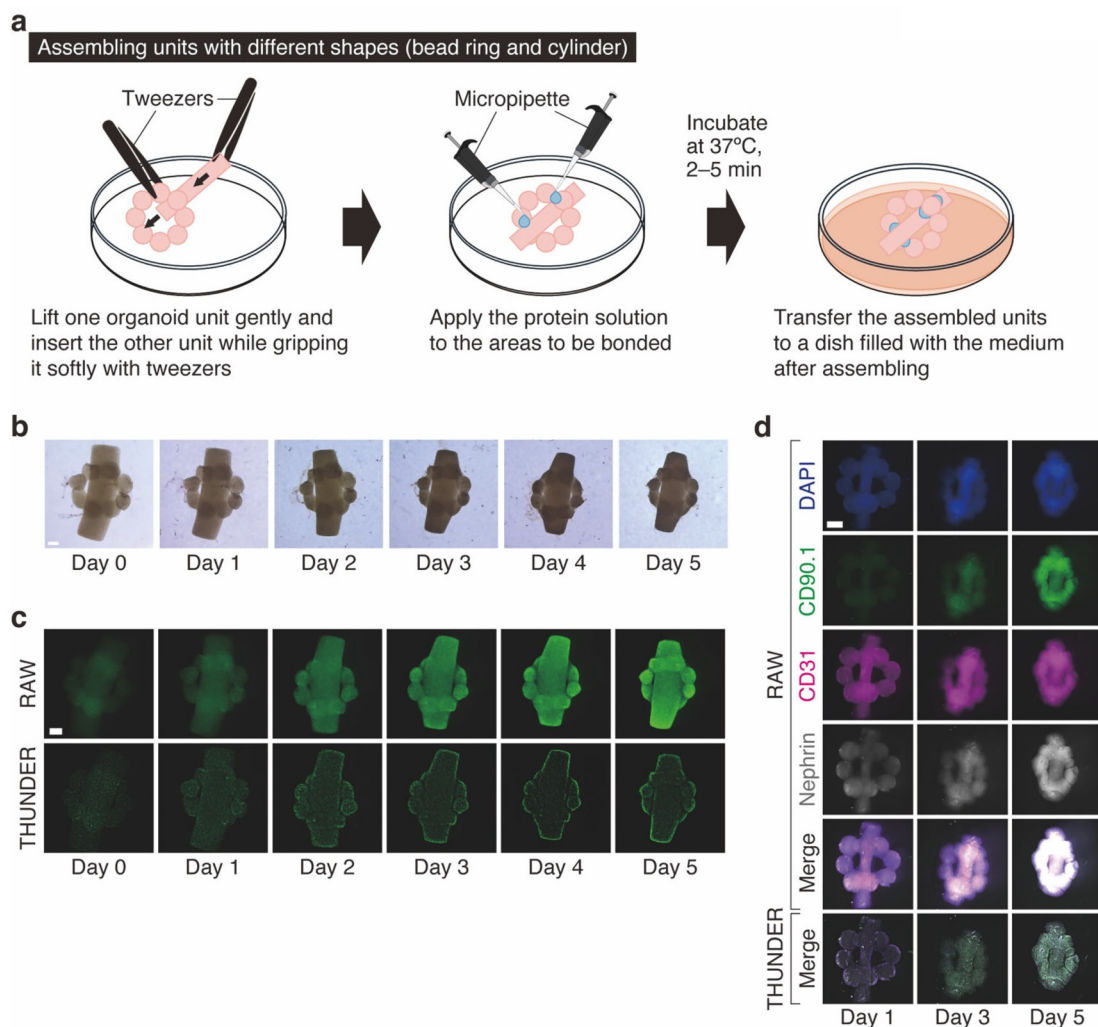
FIG. 5. Assembly of organoid units with different geometries. (a) Overview of how to assemble the organoid units with different geometries. (b) Time-sequenced brightfield images of the assembled MDA-MB-231 organoid units ($n = 3$). Scale bar, 1 mm. (c) Live fluorescence images of the assembled MDA-MB-231 organoid units, expressing GFP in the cytoplasm ($n = 3$). *Upper row*: wide-field fluorescence images (raw data), *lower row*: images processed by the THUNDER imaging system with instant computational clearing (ICC) and extended depth of field (EDF). Scale bars, 1 mm. (d) Representative fluorescence-stained images of the assembled human-kidney glomerular tissue-like organoid units ($n = 3$). Each marker protein is stained on three cell types: NHMCs (CD90.1), HUVECs (CD31), and HRGEpCs (Nephrin). *Upper 5 rows*: wide-field fluorescence images (raw data), *lower row*: images processed by the THUNDER imaging system with instant computational clearing (ICC) and extended depth of field (EDF). Scale bar, 1 mm.

monoclonal anti-CD31 antibody (Cat# 3528) was purchased from Cell Signaling Technology (Danvers, MA, USA). The FITC-conjugated human monoclonal anti-CD90.1 antibody (Cat# 130-112-683) was purchased from Miltenyi Biotec (Bergisch Gladbach, Germany). Alexa Fluor 594-conjugated goat anti-mouse IgG (Cat# A-11032) and Alexa Fluor 647-conjugated donkey anti-sheep IgG (Cat# A-21448) secondary antibodies were purchased from Thermo Fisher Scientific.

The dilution concentrations of antibodies used in immunohistochemistry and immunofluorescence staining were as follows: nephrin, 5 μg/ml; CD31, 1:500; CD90.1, 1:30; secondary antibodies, 1:200. The primary antibodies against CD90.1, CD31, and nephrin label NHMCs, HUVECs, and HRGEpCs, respectively.

Immunohistochemistry

Cultured organoid units were fixed with 4% paraformaldehyde phosphate buffer saline (PFA; 163-20145, Fujifilm Wako Pure Chemical Corp.) for 1 h at room temperature (RT). The units were cryoprotected by soaking in 20% sucrose/phosphate buffered saline (PBS; 05913, Nissui Pharmaceutical, Tokyo, Japan) for 5 h and 30% sucrose/PBS for an additional overnight at 4 °C. Fixed units were frozen in optical cutting temperature (OCT) compound (45833, Sakura Finetek Japan, Tokyo, Japan) and cut into 15 μm-thick frozen sections on cryofilm using a cryostat (CM1860, Leica Microsystems). After cutting out the frozen sections, the cells were permeabilized with 0.1% Triton X-100 (17-1315-01, Pharmacia Biotech, Uppsala, Sweden) in
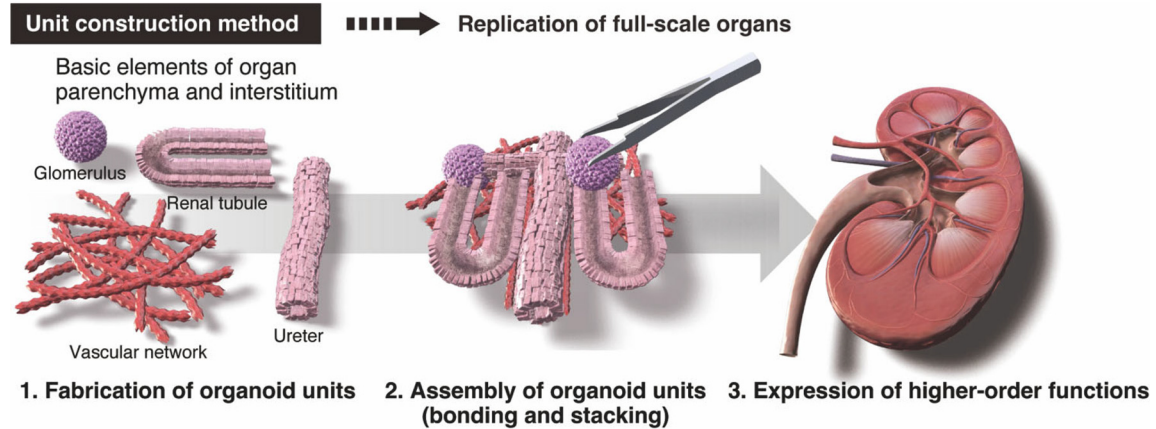
FIG. 6. Concept of the proposed unit construction method for replication of full-scale organs with organoids.

PBS, followed by incubation in 1% Block Ace (BA; UKB40, KAC, Kyoto, Japan) in PBS to prevent nonspecific antibody absorption. The cells were then stained using the primary and secondary antibodies diluted in 1% BA in PBS and PBS, respectively. Cell nuclei were stained using 4′,6-diamidino-2-phenylindole (DAPI; D1306, Invitrogen, Thermo Fisher Scientific). Stained organoid unit sections were observed with optical sectioning fluorescence microscopy (Axio Observer 7 with Apotome 3, Carl Zeiss, Oberkochen, Germany).
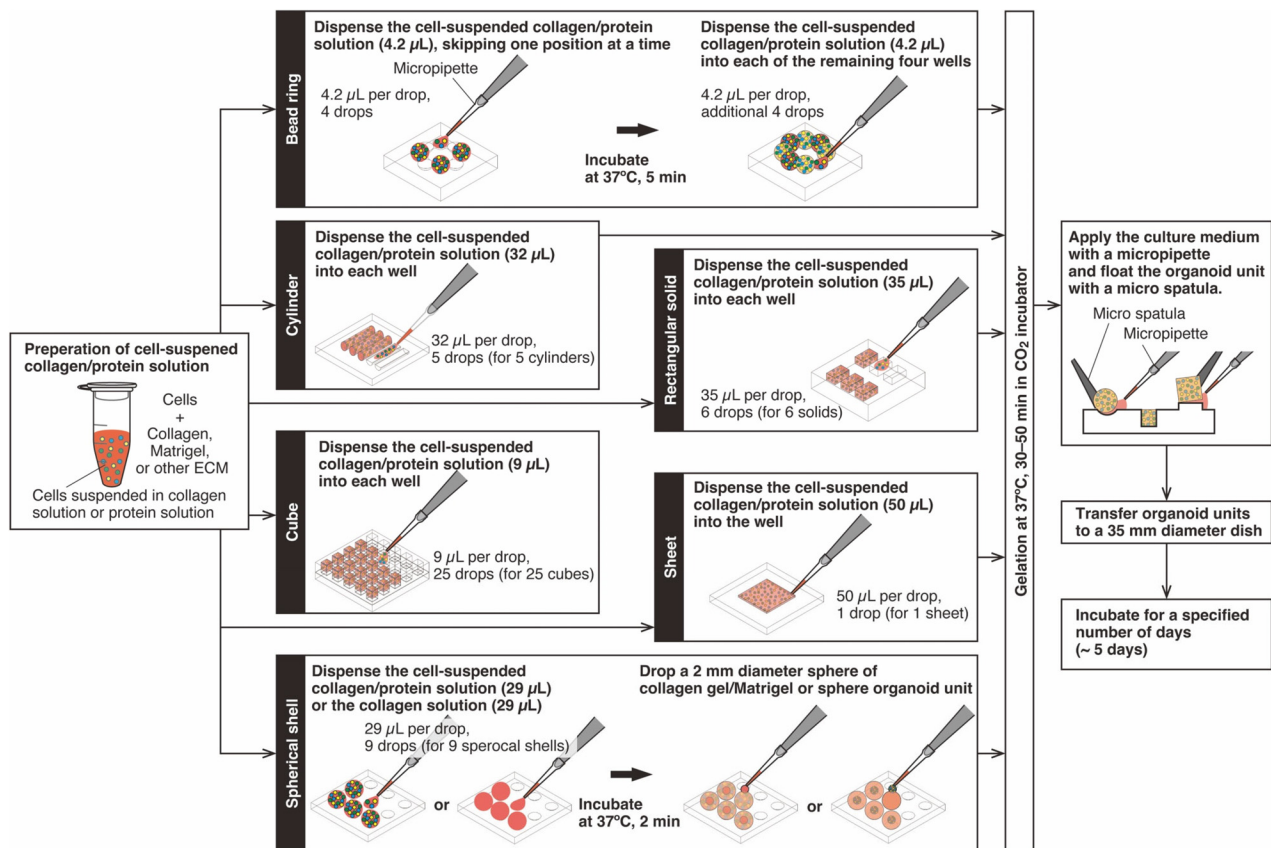

FIG. 7. Procedure for fabrication of organoid units with each geometry. Cell-suspended collagen/protein solution was prepared on ice to give the final concentration of 5.0×10^6 cells/ml in this study.

Immunofluorescence staining

Cultured organoid units were fixed with 4% PFA for 1 h. For multiplex staining with antibodies, the samples were made transparent. After fixation, the units were immersed overnight in 50% Tissue-Clearing Regent CUBIC-L (T3740, Tokyo Chemical Industry, Tokyo, Japan) containing 500 mM NaCl, followed by membrane permeabilization and blocking with 0.15% Triton-X100 and 1% BA in PBS for 1 h. The cells were stained overnight at 4 °C with primary antibodies (diluted in 1% BA in PBS) and secondary antibodies (diluted in PBS), respectively, and then post-fixed with 4% PFA for 1 h. Cell nuclei were also stained with DAPI. The stained units were soaked in 50% Tissue-Clearing Reagent CUBIC-R+(N) (T3983, Tokyo Chemical Industry) for 20 min and observed in 100% CUBIC-R+(N). Unless otherwise noted, the staining process was performed at RT, with three 15-min washes with PBS between each step. All processes were carried out with shaking. Fluorescence images of the stained units were obtained with the fluorescence imaging system or optical sectioning fluorescence microscopy.

Live/dead assay

The cell death in the organoid units was quantitatively evaluated using an Apoptotic, Necrotic, and Healthy Cells Quantification Kit (30018, Biotium, CA, USA) according to the manufacturer's instructions. The 2 mm-diameter spherical organoid units prepared with MDA-MB-231 or HRGEpC were washed with PBS with Mg^{2+} and Ca^{2+} thrice, followed by incubation with the staining solution containing FITC-Annexin V, Ethidium homodimer III, and Hoechst 33342 for 30 min at 37 °C. The cells were then washed with the PBS with Mg^{2+} and Ca^{2+} thrice, and fixed with PFA containing 1.25 mM $CaCl_2$ for an hour. The stained cells were covered with the PBS with Mg^{2+} and Ca^{2+} after washing out PFA. We observed their fluorescence using the fluorescence imaging system. MDA-MB-231 cells are a stable GFP-expressing cell line and, therefore, could not be labeled with FITC-Annexin V and were only stained with Hoechst and Ethidium homodimer III.

Data quantification

To measure the overall changes, i.e., morphological changes, in organoid units, we monitored their area, perimeter, height, and major and minor axes based on stereomicroscopic images using ImageJ Fiji.[45] In the cases of bead ring, sphere, and spherical shell units, their diameters (i.e., major and minor axes) were obtained by a computation based on an ellipse equivalent to the outline shape. For the bead shape units, the major and minor axes of the outer and inner circumferences were measured, respectively. For the spherical shell units, the major and minor axes of the outer and inner spheres were measured, respectively.

To evaluate the spatial relationship among different cell types within the organoid unit, which contains a large number of cells, we used the standard index of co-localization, the Pearson's correlation coefficient.[46,47] The correlation coefficient was obtained from the optical sectioning fluorescence microscopy data using ImageJ Fiji's "Coloc 2" function.

Data reproducibility

All values are shown as mean ± standard deviation (SD) unless stated otherwise. Data were obtained from at least three independently repeated experiments.

SUPPLEMENTARY MATERIAL

See the supplementary material for the details of the molds used to fabricate the organoid units, the conditions for milling them, and the descriptions of supplementary movies.

AUTHOR DECLARATIONS
Conflict of Interest

The authors have no conflicts to disclose.

Ethics Approval

Ethics approval is not required.

Author Contributions

Ayaka Kadotani: Conceptualization (equal); Investigation (lead); Methodology (lead); Validation (lead); Visualization (lead); Writing – original draft (equal); Writing – review & editing (equal). **Gen Hayase:** Funding acquisition (supporting); Resources (supporting); Supervision (supporting); Writing – review & editing (equal). **Daisuke Yoshino:** Conceptualization (equal); Funding acquisition (lead); Methodology (supporting); Project administration (lead); Resources (lead); Supervision (lead); Validation (supporting); Visualization (supporting); Writing – original draft (equal); Writing – review & editing (equal).

DATA AVAILABILITY

The data that support the findings of this study are available within the article and its supplementary material.

REFERENCES

[1] J. Kim, B. K. Koo, and J. A. Knoblich, "Human organoids: Model systems for human biology and medicine," Nat. Rev. Mol. Cell Biol. **21**, 571–584 (2020).

[2] M. Takasato, P. Er, H. Chiu et al., "Kidney organoids from human iPS cells contain multiple lineages and model human nephrogenesis," Nature **526**, 564–568 (2015).

[3] M. Lancaster, M. Renner, C. A. Martin et al., "Cerebral organoids model human brain development and microcephaly," Nature **501**, 373–379 (2013).

[4] K. McCracken, E. Catá, C. Crawford et al., "Modelling human development and disease in pluripotent stem-cell-derived gastric organoids," Nature **516**, 400–404 (2014).

[5] C. Watson, M. Mahe, J. Múnera et al., "An in vivo model of human small intestine using pluripotent stem cells," Nat. Med. **20**, 1310–1314 (2014).

[6]B. R. Dye, D. R. Hill, M. H. Ferguson et al., "In vitro generation of human pluripotent stem cell derived lung organoids," eLife 4, e05098 (2015).

[7]M. Bleijs, M. van de Wetering, H. Clevers, and J. Drost, "Xenograft and organoid model systems in cancer research," EMBO J. 38, e101654 (2019).

[8]J. Qu, F. S. Kalyani, L. Liu, T. Cheng, and L. Chen, "Tumor organoids: Synergistic applications, current challenges, and future prospects in cancer therapy," Cancer Commun. 41, 1331–1353 (2021).

[9]M. Bershteyn, T. J. Nowakowski, A. A. Pollen, E. Di Lullo, A. Nene, A. Wynshaw-Boris, and A. R. Kriegstein, "Human iPSC-derived cerebral organoids model cellular features of lissencephaly and reveal prolonged mitosis of outer radial glia," Cell Stem Cell 20, 435–449 (2017).

[10]S. Choi, Y. Kim, M. Hebisch et al., "A three-dimensional human neural cell culture model of Alzheimer's disease," Nature 515, 274–278 (2014).

[11]C. Gonzalez, E. Armijo, J. Bravo-Alegria et al., "Modeling amyloid beta and tau pathology in human cerebral organoids," Mol. Psychiatry 23, 2363–2374 (2018).

[12]A. Taguchi and R. Nishinakamura, "Higher-order kidney organogenesis from pluripotent stem cells," Cell Stem Cell 21, 730–746 (2017).

[13]I. T. Ozbolat and M. Hospodiuk, "Current advances and future perspectives in extrusion-based bioprinting," Biomaterials 76, 321–343 (2016).

[14]Z. Xia, S. Jin, and K. Ye, "Tissue and organ 3D bioprinting," SLAS Technol. 23, 301–304 (2018).

[15]R. Choudary, N. Saini, D. S. Chopra, D. Singh, and N. Singh, "A comprehensive review of 3D printing biomaterials: Properties, strategies and wound healing application," J. Mater. Res. 38, 3264–3300 (2023).

[16]H. Q. Xu, J. C. Liu, Z. Y. Zhang, and C. X. Xu, "A review on cell damage, viability, and functionality during 3D bioprinting," Military Med. Res. 9, 70 (2022).

[17]S. You, Y. Xiang, H. H. Hwang et al., "High cell density and high-resolution 3D bioprinting for fabricating vascularized tissues," Sci. Adv. 9, eade7923 (2023).

[18]B. E. Kelly, I. Bhattacharya, H. Heidari, M. Shusteff, C. M. Spadaccini, and H. K. Taylor, "Volumetric additive manufacturing via tomographic reconstruction," Science 363, 1075–1079 (2019).

[19]P. N. Bernal, P. Delrot, D. Loterie et al., "Volumetric bioprinting of complex living-tissue constructs within seconds," Adv. Mater. 31, e1904209 (2019).

[20]D. Ribezzi, M. Gueye, S. Florczak et al., "Shaping synthetic multicellular and complex multimaterial tissues via embedded extrusion-volumetric printing of microgels," Adv. Mater. 35, 2301673 (2023).

[21]K. J. Wolf, J. D. Weiss, S. G. M. Uzel, M. A. Skylar-Scott, and J. A. Lewis, "Biomanufacturing human tissues via organ building blocks," Cell Stem Cell 29, 667–677 (2022).

[22]J. G. Roth, L. G. Brunel, M. S. Huang et al., "Spatially controlled construction of assembloids using bioprinting," Nat. Commun. 14, 4346 (2023).

[23]M. A. Skylar-Scott, S. G. M. Uzel, L. L. Nam et al., "Biomanufacturing of organ-specific tissues with high cellular density and embedded vascular channels," Sci. Adv. 5, 2aaw2459 (2019).

[24]J. A. Brassard, M. Nikolaev, T. Hübscher, M. Hofer, and M. P. Lutolf, "Recapitulating macro-scale tissue self-organization through organoid bioprinting," Nat. Mater. 20, 22–29 (2021).

[25]Y. Iijima, N. Uenaka, M. Morimoto et al., "Biological characterization of breast cancer spheroid formed by fast fabrication method," In Vitro Models 3, 19–32 (2024).

[26]Z. Zhao, X. Chen, A. M. Dowbaj et al., "Organoids," Nat. Rev. Methods Primers 2, 94 (2022).

[27]R. J. McMurtrey, "Analytic models of oxygen and nutrient diffusion, metabolism dynamics, and architecture optimization in three-dimensional tissue constructs with applications and insights in cerebral organoids," Tissue Eng., Part C 22, 221–249 (2016).

[28]M. Lancaster and J. A. Knoblich, "Organogenesis in a dish: Modeling development and disease using organoid technologies," Science 345, 1247125 (2014).

[29]Y. Shi, L. Sun, M. Wang et al., "Vascularized human cortical organoids (vOrganoids) model cortical development in vivo," PLoS Biol. 18, e3000705 (2020).

[30]The Human Protein Atlas, see https://www.proteinatlas.org/ENSG00000154096-THY1/tissue/kidney#multiplex for "Kidney," Accessed September 1, 2024.

[31]G. D. Cascarano, F. S. Debitonto, R. Lemma et al., "A neural network for glomerulus classification based on histological images of kidney biopsy," BMC Med. Inf. Decis. Making 21, 300 (2021).

[32]B. B. Lake, R. Menon, S. Winfree et al., "An atlas of healthy and injured cell states and niches in the human kidney," Nature 619, 585–594 (2023).

[33]B. Zohar, Y. Blinder, D. J. Mooney, and S. Levenberg, "Flow-induced vascular network formation and maturation in three-dimensional engineered tissue," ACS Biomater. Sci. Eng. 4, 1265–1271 (2018).

[34]C. O'Connor, E. Brady, Y. Zheng et al., "Engineering the multiscale complexity of vascular networks," Nat. Rev. Mater. 7, 702–716 (2022).

[35]P. Jain, H. Kathuria, and N. Dubey, "Advances in 3D bioprinting of tissues/organs for regenerative medicine and in-vitro models," Biomaterials 287, 121639 (2022).

[36]N. M. Wragg, L. Burke, and S. L. Wilson, "A critical review of current progress in 3D kidney biomanufacturing: Advances, challenges, and recommendations," Renal Replacement Ther. 5, 18 (2019).

[37]R. Levato, T. Jungst, R. G. Scheuring, T. Blunk, J. Groll, and J. Malda, "From shape to function: The next step in bioprinting," Adv. Mater. 32, e1906423 (2020).

[38]H. Cui, M. Nowicki, J. P. Fisher, and L. G. Zhang, "3D bioprinting for organ regeneration," Adv. Healthcare Mater. 6, 1601118 (2017).

[39]I. T. Ozbolat, "Bioprinting scale-up tissue and organ constructs for transplantation," Trends Biotechnol. 33, 395–400 (2015).

[40]D. E. Discher, P. Janmey, and Y. L. Wang, "Tissue cells feel and respond to the stiffness of their substrate," Science 310, 1139–1143 (2005).

[41]V. Vogel and M. Sheetz, "Local force and geometry sensing regulate cell functions," Nat. Rev. Mol. Cell Biol. 7, 265–275 (2006).

[42]D. Jaalouk and J. Lammerding, "Mechanotransduction gone awry," Nat. Rev. Mol. Cell Biol. 10, 63–73 (2009).

[43]J. Eyckmans, T. Boudou, X. Yu, and C. S. Chen, "A hitchhiker's guide to mechanobiology," Dev. Cell 21, 35–47 (2011).

[44]G. Hayase and D. Yoshino, "CNC-milled superhydrophobic macroporous monoliths for 3D cell culture," ACS Appl. Bio Mater. 3, 4747–4750 (2020).

[45]J. Schindelin, I. Arganda-Carreras, E. Frise et al., "Fiji: An open-source platform for biological-image analysis," Nat. Methods 9, 676–682 (2012).

[46]K. W. Dunn, M. M. Kamocka, and J. H. McDonald, "A practical guide to evaluating colocalization in biological microscopy," Am. J. Physiol. Cell Physiol. 300, C723–742 (2011).

[47]A. Li, S. Muenst, J. Hoffman et al., "Mesenchymal-endothelial nexus in breast cancer spheroids induces vasculogenesis and local invasion in a CAM model," Commun. Biol. 5, 1303 (2022).